

given by $R' = (A_2^2 - \rho^2) / (K_H^{**2} - K^{*2}) \simeq 0.95$. If the mixing is relatively important, the result now includes¹⁰ two mixing angles $\theta_{K^*K^{**}}$ and $\theta_{K_H^{**}K_H^{***}}$. However, as in the case of the R we expect that R' will not deviate very significantly from the $SU(3)$ value. From the reported value¹ $\Gamma(A_{2H} \rightarrow \rho\pi) \simeq 29$ MeV, $R' \simeq 1$ predicts $\Gamma(K_H^{**} \rightarrow K^*\pi) \simeq 12$ MeV, whereas experimentally $\Gamma(K^{**}(1420) \rightarrow K^*\pi) \simeq 30$ MeV. Therefore, if we identify the $K^{**}(1420)$ solely with the K_H^{**} we are faced with a large $SU(3)$ breaking which our $SU(3)$ approximation cannot explain. However, our $SU(3)$ approximation predicts that the $K^{**}(1420)$ is the overlap of the two resonances, K_H^{**} and K_L^{**} , and the combined width $\Gamma(K_H^* \rightarrow K^*\pi) + \Gamma(K_L^{**} \rightarrow K^*\pi)$ is not far

¹⁰ R' is given by

$$R' = (K^{*2} - K^{*2}) (A_2^2 - \rho^2) (K_H^{**2} - K^{*2} - A_2^2 + \rho^2)^{-1} \\ \times (K_H^{**2} - K^{*2})^{-1} \cos\theta_{K^*K^{**}} (\cos\theta_{K_H^{**}K_H^{***}})^{-1}.$$

The case of no mixing is obtained by setting $K^{*2} \rightarrow \infty$ and $\theta_{K^*K^{**}} = \theta_{K_H^{**}K_H^{***}} = 0$.

from the observed one, $\Gamma(K^{**} \rightarrow K^*\pi) \simeq 30$ MeV.¹¹ This is quite satisfactory.

As regards the $I=0$ 1^- mesons, we may have two, ω' and ϕ' , which can also mix. There is no simple argument for the degeneracy between the (f, f') and the (ω', ϕ') unless we add more assumptions. The decay $1^- \rightarrow 0^- + 0^-$ is forbidden in the $SU(3)$ limit. Therefore, the decay $K_L^{**} \equiv K^{*'} \rightarrow K\pi$ will not be important compared with the mode $K^{*'} \rightarrow K^*\pi$. Consequently, the $K^{**}(1420) \rightarrow K^*\pi$ decay can be predominantly due to the $K_H^{**} \rightarrow K^*\pi$ decay.

ACKNOWLEDGMENT

We thank Professor G. Snow for reading the manuscript and for useful suggestions.

¹¹ From the naive point of view of reasonable $SU(3)$ breaking, Harari also mentioned the possible splitting of the K^{**} . H. Harari, in *Proceedings of the Fourteenth International Conference on High-Energy Physics, Vienna, 1968* (CERN, Geneva, 1968), p. 195.

Proton-Proton Triple Scattering at 1.9 GeV*

W. C. CARITHERS, JR.,† R. K. ADAIR, C. J. B. HAWKINS‡
Yale University, New Haven, Connecticut 06520

AND

H. KASHA, R. C. LARSEN, L. B. LEIPUNER, L. W. SMITH, AND T. P. WANGLER§
Brookhaven National Laboratory, Upton, New York 11973

(Received 12 September 1968)

We have measured the Wolfenstein triple-scattering parameters R , D , and A' at 1.9 GeV for p - p scattering at 90° in the c.m. system. We find that $R = 0.11 \pm 0.16$, $A' = -0.54 \pm 0.16$, and $D = 0.91 \pm 0.21$, where these parameters are defined in the c.m. system. The possibility of a vector character for the strong interactions is discussed. We conclude that neither a single vector-meson exchange nor a single pseudoscalar-meson exchange can account for the data. Spin effects are found to remain an important part of the nucleon-nucleon interaction at four-momentum transfer $-t = 1.8$ (GeV/c)².

I. INTRODUCTION

THE nucleon-nucleon scattering problem has been studied extensively as a logical starting point for a quantitative understanding of nuclear forces. At low energies the interaction is complicated: The scattering amplitude generally depends upon both the initial and final spin configurations as well as the initial and final momenta. A complete description of the scattering at a definite angle and energy then requires a determination of the spin correlations, which in turn re-

quires the equivalent of a set of triple-scattering experiments. Previously nucleon-nucleon triple-scattering experiments have been performed at energies accessible to the high-energy cyclotrons—typically at energies up to 400 MeV—in an attempt to understand the important and complicated spin-dependent effects of nuclear forces.¹ The extension of such measurements to higher energies, as in the present experiment, thus becomes intrinsically interesting.

At high momentum transfers, the triple-scattering experiments might be expected to exhibit some evidence of an asymptotic simplicity of the nucleon-nucleon interactions. We might find that the complicated low-energy structure is essentially a surface effect which

* Work performed under the auspices of the U. S. Atomic Energy Commission.

† Present address: Nevis Laboratory, Columbia University, Irvington, N. Y.

‡ Present address: Nuclear Physics Department, Oxford University, Oxford, England.

§ Present address: Argonne National Laboratory, Argonne, Ill.

¹ For a review, see M. H. MacGregor, M. J. Moravcsik, and H. P. Stapp, *Ann. Rev. Nucl. Sci.* **10**, 291 (1960).

would approach a very simple limit at small distances or high momentum transfers. For the sake of definiteness we consider the results which might be expected from each of three simple models of the interaction at high momentum transfer. We might find that the interaction is so complex that the nucleons lose all knowledge of their initial spin direction and there are no spin correlations, or perhaps we will find that at high momentum transfers the interaction is dominated by single-meson exchange. Just as one pion exchange dominates the low-momentum-transfer interaction, a single-meson-exchange model might continue to show a pseudoscalar character, or perhaps we will find that the interaction is dominated by vector-meson exchange. For essentially aesthetic reasons, a vector-meson-dominance model seems especially attractive.

Of the three interactions which are important on a microscopic level, two are known to transform like a vector. The weak interactions can be adequately described, at least phenomenologically, by the $V-A$ interaction. At present there is no experimental evidence that our understanding of the electromagnetic interaction is not complete. The quantum electrodynamic description of a charged vector current interacting via the vector photon seems to work even down to the smallest distances yet studied. The structure of the strong interactions is not well understood, but it is attractive to speculate that the strong interaction might also be essentially vector in character, even as the electromagnetic (em) interaction and the weak interaction.

We might consider such a model in analogy with the electromagnetic case. When a charged particle enters a uniform transverse magnetic field it describes a circular orbit with the familiar cyclotron frequency $\omega_c = (e/m)H$. The spin-precession frequency is just $\omega_s = \mu H$, where $\mu = g(e/m)\sigma$. An important result of Dirac theory states that $g=2$ so that the cyclotron frequency and the spin-precession frequency are equal. Hence, the spin and momentum directions precess together and the component of the spin along the momentum is conserved. We shall call this conserved quantity $\sigma \cdot \hat{p}$, or the helicity.

Helicity is conserved in the scattering of highly relativistic electrons from a Coulomb field. The Coulomb field is transformed essentially into a magnetic field in the rest system of the electron, and helicity conservation follows from the equivalence of spin- and momentum-precession frequencies. Formally, this result can be regarded as a consequence only of the Dirac equation and the minimal vector character of the em interaction. If we regard the vector structure as fundamental, then the theory could be extended so that our results should obtain for any weak vector field. The em case would then be a special case for which the coupling strength is $\alpha=1/137$ and the photon has zero mass. We shall investigate the possibility that under certain conditions the strong interactions have such a

vector structure which is manifest as an approximate conservation of helicity.

However, even the electron is not a bare Dirac particle. When the photon field is turned on, the electron can emit and reabsorb photons. These processes renormalize the bare mass and the magnetic moment; hence, the spin-precession frequency is no longer exactly equal to the cyclotron frequency for the physical particle. For the electron ($g-2$) is of the order of α .

For the strongly interacting nucleon such effects are much larger and more important. The nucleon can emit and reabsorb mesons as well as undergo second-order processes involving baryon-antibaryon pairs. The consequential distribution of charges presumably modifies the bare magnetic moment: $g=5.59$ for the proton. These meson cloud effects are not small in the usual sense, nor are they particularly simple. They are responsible for the rich complexity of low-energy phenomena including nuclear physics. However, if we can penetrate below such surface effects to the point where the bare nucleon dominates, we can hope that the simplicity of a Dirac particle moving in a weak vector field will emerge. Hence, if the bare-nucleon interaction is essentially a vector interaction, we would expect helicity to be approximately conserved for large momentum transfers. To establish a scale we might consider momentum transfers of the order of the nucleon mass which would be conjugate to the nucleon Compton wavelength.

At small momentum transfers, the nucleon-nucleon interaction appears to have a pseudoscalar character. This is equivalent to a single-pion-exchange model, which works well for distances larger than about two-pion Compton wavelengths. Regarding the vector character as more fundamental we would consider the long-range pion to consist of a pair of tightly bound vector mesons. At large momentum transfers the vector mesons would be exchanged directly.

The simple consequence of helicity conservation which results from the exchange of a single vector meson in the limit of high momentum transfer is seriously modified, even within the limits of a vector-dominance model, if the vector interaction is so strong that several vector mesons are exchanged. The momentum transfer at each exchange may not, then, be large; and since the relativistic limit will not be approached, complete helicity conservation will not occur.

If the interaction is dominated by an exchange of one pseudoscalar meson, the helicity of the nucleons will be reversed in the relativistic limit. Thus, if a pseudoscalar meson is exchanged, before or after a vector meson is exchanged, the helicity will tend to be flipped provided the momentum transfer for both exchanges is large compared to the masses of the particles involved. This kind of initial- or final-state interaction could complicate the results considerably even if the

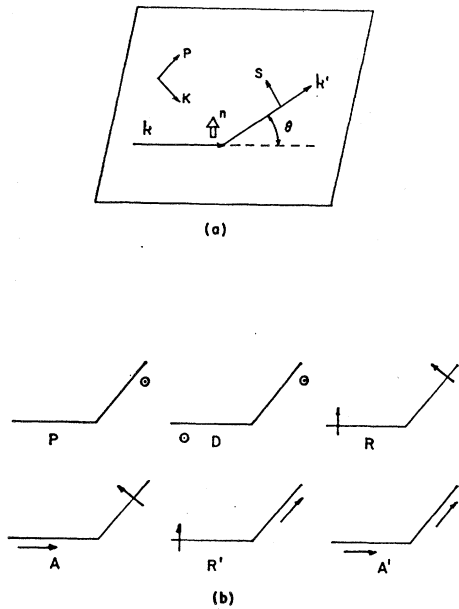


FIG. 1. (a) Coordinate system. (b) Schematic representation of Wolfenstein parameters.

basic vector-dominance concept were valid; but two such large momentum transfers would not seem to be possible at the energies reached in the experiment.

It is also possible that the high-momentum-transfer interactions are very complex, involving the exchanges of many particles, and that spin information is distributed among many degrees of freedom and effectively lost. We would then expect to see no strong spin correlations. As we mentioned above, even such a result would not exclude a vector-dominance model as the exchange of many vector mesons would destroy spin correlations even as the exchange of very many mesons of any kind would result in the loss of the spin information.

From each of these models—single vector-meson exchange, single pseudoscalar-meson exchange, and the complex interaction model where the spin-direction information is lost—we can deduce specific predictions for the correlations between initial and final spin directions of the interacting protons.

II. FORMALISM

To measure all of the appropriate spin correlations we must prepare polarized beams, scatter the beams with the interaction we wish to study, and finally measure the polarization magnitudes and directions after scattering. To this extent, the experiment is a standard triple-scattering experiment. Since both incident and target particles have spin $\frac{1}{2}$, the complexity or number of possible configurations is large, and thus might require many parameters to describe the interaction completely. However, symmetry requirements

restrict the number of possible states, and hence the number of parameters.

Wolfenstein has studied various parametrizations of the scattering process. These are adequately described in the literature,² and we will present only the results of the formalism leading to those parameters which we measure. With one important exception, we employ the notation developed by Wolfenstein and Ashkin and by Stapp.^{3,4} We have departed from the standard definition of the Wolfenstein parameters in the lab system by defining all parameters in the c.m. system to take full advantage of the simplicity imposed by symmetry. Wolfenstein has shown that the triple-scattering process can be described by the polarization P , plus five parameters— D , A , R , A' , and R' —which bear his name.² They are defined by

$$I\langle\sigma\rangle = I_0 \{ [P + D\langle\sigma\rangle_i \cdot \hat{n}] \hat{n} + [A\langle\sigma\rangle_i \cdot \hat{k} + R\langle\sigma\rangle_i \cdot (\hat{n} \times \hat{k})] \hat{S} + [A'\langle\sigma\rangle_i \cdot \hat{k} + R'\langle\sigma\rangle_i \cdot (\hat{n} \times \hat{k})] \hat{k}' \},$$

where I_0 is the incident intensity, \hat{k} is a unit vector along the incoming momentum, \hat{k}' is a unit vector along the outgoing momentum, and in the standard geometry \hat{n} , \hat{S} , \hat{K} , and \hat{P} are unit vectors along $\hat{k} \times \hat{k}'$, $\hat{n} \times \hat{k}'$, $\mathbf{k} - \mathbf{k}'$, and $\mathbf{k} + \mathbf{k}'$, respectively. These are illustrated schematically in Fig. 1. These parameters are most convenient for characterizing the experimental results, since they correspond to the experimentally prepared initial spin states and measured final spin states. For a theoretical characterization of the data the phase-shift analysis used at low energies becomes impractical, and we prefer to analyze our results directly in terms of the spin amplitudes.

The scattering process will be represented by a matrix M , to be considered an operator which acts on the initial spin state, transforming it into the final spin state:

$$|S_f\rangle = M |S_i\rangle.$$

The system can be specified by the spins of the beam and target particle, and the initial and final momenta of either particle:

$$M = M(\sigma_1, \sigma_2, k_i, k_f).$$

We work at fixed momenta and study the M matrix as an operator on the spin space of the two particles. The symmetries of identical particles at 90° in the c.m. system are most apparent in a singlet-triplet representation, where only singlet and triplet spin-flip scattering contribute. The three nonvanishing amplitudes are defined by

$$\begin{aligned} M_{10} &= \langle S_1^+ | M | S_1^0 \rangle, & \text{triplet} \\ M_{01} &= \langle S_1^0 | M | S_1^+ \rangle, & \text{triplet} \\ M_{00} &= \langle S_0^0 | M | S_0^0 \rangle, & \text{singlet.} \end{aligned}$$

² L. Wolfenstein, *Ann. Rev. Nucl. Sci.* **6**, 43 (1956).

³ L. Wolfenstein and J. Ashkin, *Phys. Rev.* **85**, 947 (1952).

⁴ H. P. Stapp, Ph.D. thesis, Lawrence Radiation Laboratory Report No. UCRL-3098, 1955 (unpublished).

A straightforward calculation gives the Wolfenstein parameters in terms of the singlet and triplet spin amplitudes:

$$I = \frac{1}{2}|M_{10}|^2 + \frac{1}{2}|M_{01}|^2 + \frac{1}{4}|M_{ss}|^2,$$

$$P, A, R' = 0, \quad ID = -\text{Re}(M_{10}M_{01}^*),$$

$$IR = (1/\sqrt{2}) \text{Re}(M_{01}M_{ss}^*),$$

$$IA' = -(1/\sqrt{2}) \text{Re}(M_{10}M_{ss}^*).$$

In terms of the models discussed above, a simple calculation shows that a helicity-conservation model, or vector-meson exchange in a relativistic limit, implies a relation between the singlet and one of the triplet amplitudes: $M_{ss} = -\sqrt{2}M_{10}$. The sign is reversed in a pseudoscalar-meson exchange, or helicity reversal, model.

III. EXPERIMENTAL DESIGN

A. Beam

The experimental design requires both transverse and longitudinally polarized beams. The Cosmotron external proton beam is unpolarized, but the spin-orbit term of the nucleon-nucleon interaction causes a scattered beam in general to acquire a net polarization. The geometry for such a scattering is shown in Fig. 1, where \mathbf{k} is the incident momentum, \mathbf{k}' is the final momentum, and θ is the scattering angle. The polarization direction lies along the direction $\mathbf{n} = \mathbf{k} \times \mathbf{k}'$. Thus, particles scattered to left have their spins pointing preferentially up, particles scattered to the right have their spins polarized down. If we consider a rotation of the diagram in Fig. 1 of 180° about the \mathbf{k} axis, it is clear that rotational invariance requires

$$I_{\text{spin up}}(\theta) = I_{\text{spin down}}(-\theta).$$

Therefore, we can reverse the sign of the polarization without changing its magnitude by reversing the scattering angle. When we reverse the scattering angle, all polarization effects (asymmetries) should change sign. By subtracting data with the opposite sign, all non-polarization effects should cancel to first order while the polarization effects add, thereby greatly improving the signal-to-background ratio. Since the polarization effects are generally small such signal enhancement is virtually a requirement.

The entire beam layout is shown in Fig. 2(a). The beam transport system serves to precess the spin direction into the transverse and longitudinal configurations needed to measure D , R , and A' . The spin directions at various points in the beam are illustrated in Fig. 2(c) as a function of the magnet polarities.

We chose to reverse the scattering angle by reversing the angle of incidence so that the scattered beam is always taken in the same direction. The beam position and scattering angle are determined by two bending magnets of opposite polarity as shown in Fig. 2(b).

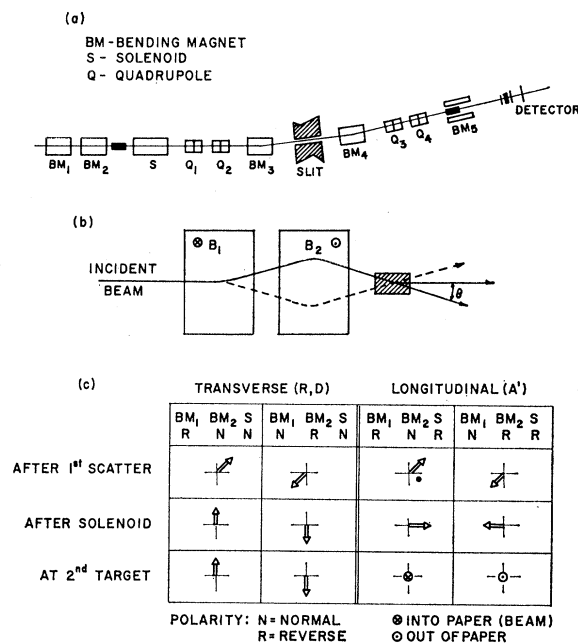


FIG. 2. (a) Beam layout. (b) Reversible angle of incidence. (c) Spin direction at various points along the beam as a function of magnet polarities.

The arrangement is such that these two magnets have approximately separate functions. The first magnet determines the beam position, or the portion of the target which is illuminated. This position is controlled and monitored by adjusting the magnet current until the beam is centered on a marked phosphorescent screen attached to the target and viewed by closed-circuit television. The target is a standard liquid- H_2 target 6 in. long and 3 in. in diam. The second bending magnet then defines the scattering angle. If we assume the magnet field survey is accurate to about 1%, then this method will define the c.m. scattering angle to about 0.1° , and hence the lab angle to about 0.04° . In any event, the error is less than the divergence of the external beam or the angular acceptance of the beam transport system and may be safely neglected. These two bending magnets, and consequently the scattering plane, are tipped at an angle of 45° with respect to the floor.

The solenoid magnet then precesses the spin direction by 45° so that the polarization is either parallel to the floor in the longitudinal case or at right angles to the floor in the transverse case. The beam is then focused with a pair of quadrupole doublets. The beam is bent through 13° in two stages on either side of a momentum-defining slit. Our acceptance solid angle is about 0.5 msr, and the momentum resolution is 2.5%. In the transverse case, the spin direction is parallel to the field of the two bending magnets so that no further precession occurs. However, in the longitudinal case the spin direction and field direction are perpendicular, and the resultant torque precesses the spin to lie along

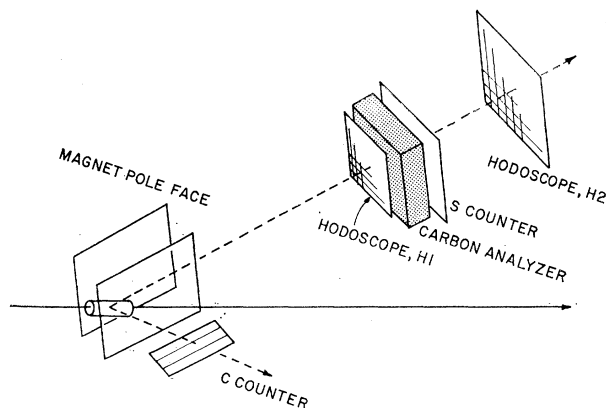


FIG. 3. Schematic representation of the detector assembly.

the beam direction. A second pair of quadrupole doublets focus the polarized beam onto the second target.

The second target is a standard liquid- H_2 target design measuring 8 in. long and 3 in. diam. This target is placed just inside the pole face of a bending magnet (BM_5) which has been tipped on its side. Parity conservation forbids direct detection of any component of polarization along the momentum direction by a single scattering.² After taking into account the polarization direction in the c.m. system and the spin rotation in the Lorentz transformation to the lab system,^{4,5} the final bending magnet precesses the spin such that the polarization direction is perpendicular to the momentum direction in the lab system to obtain the maximum analyzing efficiency.

B. Detector

The detector must select elastic scattering events at 90° in the c.m. system and measure the final polarization. The apparatus is shown schematically in Fig. 3. The scattered proton enters the first hodoscope H1 and scatters in the carbon analyzer. A second hodoscope H2 defines the carbon scattering angles. The azimuthal-angle dependence (or asymmetry) of the carbon scattering is a measure of the proton polarization. The scattered proton also passes through an efficient scintillation counter S. Using the pulse height in this counter we can discriminate against events containing more than one charged particle. The recoil proton is detected by a segmented scintillation counter C. The C counter is sufficiently long that its image for elastic events is larger than the first hodoscope, and hence it provides no fine-scale elasticity discrimination on the polar scattering angle. However, the counter is segmented in the horizontal direction and by correlating these segments with the horizontal address of the first hodoscope we obtain a measure of the coplanarity, and hence elasticity, of the final scattering.

⁴ G. Ascoli, *Z. Physik* **150**, 407 (1958).

Each hodoscope plane is a binary coded device.⁶ We consider the absence of a count in each bit to carry the same amount of information as the occurrence of a count. Each bit consists of alternate strips of Pilot B plastic scintillator and Lucite blanks. The Lucite blanks are wrapped in aluminum foil to prevent Cerenkov light or Lucite scintillations from entering the photomultiplier. Each hodoscope plane consists of 5 bits and 31 channels—a zero address is excluded. The first hodoscope is 15.5 in. square and the channel width is 0.5 in. Each bit is $\frac{1}{4}$ in. thick so each hodoscope is 2.6 in. (6.6 g/cm^2) thick. The details of the second hodoscope are the same as the first except that all linear dimensions are 1.5 times larger so the channel width is $\frac{3}{4}$ in. Each bit is viewed by a Lucite light pipe and RCA 6810A, 2-in. photomultiplier. The two least significant bits of the second hodoscope are a small exception. They are divided in two, and each half is viewed separately by a light pipe and photomultiplier. The placement of the detector relative to the target depends on the parameter to be measured. The three configurations are shown in Fig. 4. The two hodoscopes are placed so that they subtend the same solid angle with respect to the target.

The carbon analyzer consists of graphite blocks 9 in. (34 g/cm^2) thick, which cover the shadow of the first hodoscope. This carbon thickness is about 0.6 mean-free-path lengths for a proton scattering. The S counter is constructed from $\frac{3}{4}$ -in.-thick plastic scintillator viewed by a 5-in. RCA 7046 photomultiplier. A window is established on the pulse height so that large pulses coming from more than one charged particle can be rejected. This rejection allows some degree of discrimination against certain inelastic events, particularly reactions in the detector. The segmented C counter at the conjugate angle is a 2-bit, 3-channel hodoscope. Each channel is 3 in. wide and 16 in. long. The counter is placed about 25 in. away from the target. The address in the segmented counter is correlated with the horizontal address of the first hodoscope by coplanarity.

C. Logic

A rough selection of acceptable events is made with fast logic, which opens a gate to allow the data to be registered in a buffer. The fast logic is then gated off and the data is transferred from the buffer into the memory of an on-line PDP-8 computer. When the transfer is complete, the computer issues a signal to clear the buffer, and the detector is activated for the next event. All electronics are gated by a signal from the Cosmotron such that they are active only during the flat-top portion of the machine cycle. The fast logic accepts those events in which particles traverse both the detector and the segmented C counter in approximate coincidence. The S counter is used as a

⁶ L. Alvarez, *Rev. Sci. Instr.* **31**, 76 (1960).

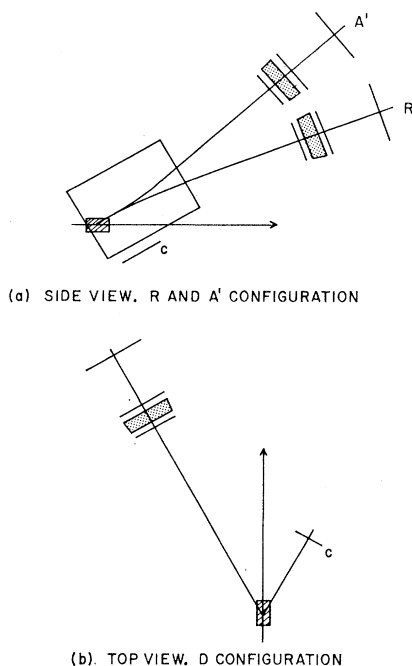


FIG. 4. Detector configurations: (a) R, A' parameter measurement. (b) D parameter measurement.

triggering criterion for particles passing through the detector, hence the low discriminator output of S provides the first part of the fast coincidence requirement. The two bits of the segmented C counter are summed with a nanocard fan-in circuit for the other part of the fast coincidence. Thus, the recoil particle can pass through any channel of this counter and still satisfy the triggering criteria.

The output of the fast coincidence circuit provides a triggering pulse for the interface logic. Upon receipt of a trigger pulse, the data-break facility of the PDP-8 takes over the automatic transfer of data from the interface buffer into core memory. The data break is a cycle-stealing operation for very fast direct transfer of data into memory. The entire transfer of one data word takes three cycles, or $4.5 \mu\text{sec}$. Each event contains 36 bits, or three words, so the total dead time is $13.5 \mu\text{sec}$. The computer issues a pulse to the interface logic to signal the completion of the data break. The interface buffer is then reset. The inhibit signals are removed from the fast coincidence and the trigger input so that the system is ready to accept the next event.

The signals from the various photomultipliers must be delayed to give the fast logic enough time to open the interface buffer gate. The photomultiplier output is clipped to a 6-nsec width. The discriminators on the fast logic are standard nanocard circuits with a 5-nsec output pulse width. The fast coincidence has a resolving time of about 10 nsec. The enable gate for the interface buffer is 20 nsec wide. The signals from all the photo-

multipliers are delayed by 25–30 ft of cable before entering the interface buffer. Each is then carefully timed in by adding the appropriate small length of cable.

The interface buffer must match the nanosecond fast logic times to the much slower microsecond computer cycle times. We decided to use the fast pulses to set a dc level (a flip-flop), which could be read and then reset by the computer itself. The buffer also contains a discriminator for rejecting noise pulses and is gated by the fast logic. At the time the experiment was designed, such a unit was not commercially available so a prototype was designed and built locally.⁷ Certain problems with cross-talk, slow gating, and poor discrimination were encountered with particular units of the initial design. Subsequent redesign eliminated the most serious problems. The situation was also improved by interposing Chronetics model 115 discriminators just before the interface buffer. These units then provided the effective discrimination and delivered a clean, standard 300-mV pulse to the interface buffer.

D. On-Line Analysis

The on-line PDP-8 computer is used primarily for writing the raw data on magnetic tape for further analysis and for monitoring the equipment performance. In addition, there is sufficient time and core length for a minimal amount of on-line analysis to check the quality of the data. The on-line processing consists of decoding the hodoscope addresses and incrementing the appropriate monitors as described below. The entire block of raw data is written on magnetic tape along with a small amount of bookkeeping information for each pulse. The program also displays a scatter plot of all the counts in each pulse on a rack-mounted oscilloscope.

Certain functions were monitored continuously during the experiment. The number of counts on each photomultiplier was monitored as an indication of tube performance. A histogram of the number of counts in each channel for both horizontal and vertical planes of each hodoscope was maintained. The on-line analysis program also monitored the quantities that would be used for rejection criteria. Inelastic events were indicated by a monitor on the number of counts which fell outside the nominal coplanarity limit. A record was also kept of the number of zero addresses in the hodoscope planes. Zero is not a legal address and indicates a failure of a coincidence count in that hodoscope plane. A monitor on the total counts from the high discriminator of the S counter provided an indication of the number of multiple particle events. Finally, we recorded monitors on the scattering in the carbon analyzer. Separate monitors were incremented when-

⁷J. Alderman, Brookhaven National Laboratory Particle Physics Research Group Internal Report No. JCA-1, 1967 (unpublished).

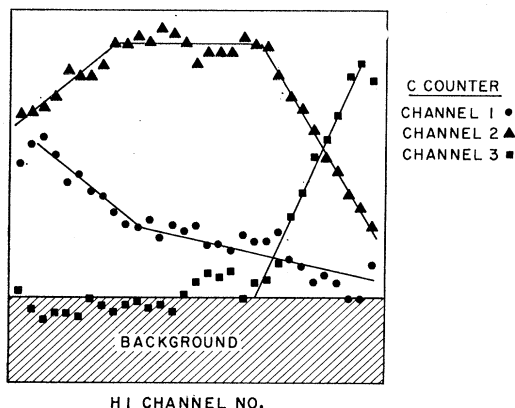


FIG. 5. Coplanarity correlations between horizontal intensity distribution for hodoscope H1 and segmented counter C.

ever the particle scattered approximately in the 3° – 6° zone to the left, right, above, and below. All monitors except the hodoscope histograms are listed automatically on the teletype every 20 min for diagnostic purposes. They are available by keyboard request at any time.

IV. ANALYSIS

The data analysis consists of extracting the asymmetry in the final scattering on carbon for those protons which scatter elastically in the second hydrogen target. The asymmetries can then be related to the Wolfenstein parameters and compared with the predictions of various models. The analysis proceeds in five steps: (1) establishment of selection criteria and rejection of unacceptable data, (2) precise determination of the 0° scattered beam direction, (3) removal of portions of the data where inefficiencies are large, (4) determination of the asymmetry by fitting a sine curve to the azimuthal angle dependence, and (5) correction for background and other small effects.

A. Selection Criteria

Except for the coincidence requirement of the fast logic, no selection of events is made on-line. The raw data are written directly onto magnetic tape. The fast logic involves no direct interrogation of the hodoscope addresses, and the geometry is such that many of the events accepted by the fast logic will miss one of the hodoscope planes entirely. If the address of any of the planes is a zero, the event is rejected in the analysis. The occurrences of a zero address, or a “miss,” are checked for correlations among the four hodoscope planes. The correlations are consistent with geometric and absorption effects.

Events are rejected whenever the pulse height from counter S of Fig. 3 exceeds an upper threshold, indicating that more than one charged particle traversed the detector. Samples of data of this kind indeed give distributions where the counting rate for each channel

is weighted by the number of bits of scintillator contained in that channel, suggesting a dominance of multiple particle events.

The data is also checked for certain types of hardware errors which appear randomly as a dropped or incorrectly set bit. Parity checks on the tape handling are built into the hardware, and all hodoscope addresses are constrained to lie within the legal limits (1–31 for the large hodoscope and 1–3 for the segmented C counter). Such errors are extremely rare, easily found and rejected, and cause no serious problems.

Protons which scatter elastically at 90° in the c.m. system must satisfy the following two requirements in the lab system: (1) The outgoing particles must emerge with the same polar scattering angle ($\theta=35^{\circ}$) and (2) all momenta must be coplanar.

The fast logic provides a rough selection on the first requirement. However, the segmented C counter is so long that its elastic image is larger than the hodoscope. When a fast coincidence is satisfied, the hodoscope address of the elastically scattered particle cannot be resolved—the coincidence itself is the only indication of scattering angle equality. However, the C counter is segmented in the azimuthal direction, and we can resolve a region of horizontal hodoscope addresses for coplanar events. In the analysis, elastic events are determined by their coplanarity. Figure 5 shows the hodoscope distributions correlated with each channel of the C counter. The background level is also indicated. For convenience in the analysis, the data is separated into two classes. The “elastic” sample includes all events which are correlated with channel 2 of the C counter. This sample is seen to have an integrated signal-to-background ratio of about 2. Events which are correlated with channels 1 and 3 of the C counter have a signal-to-background ratio of about 0.5 and are placed in the “inelastic” sample. Separate asymmetries are calculated for each sample to allow a correction to be made for the background.

To measure small asymmetries in the carbon scattering, we must know the direction that corresponds to 0° scattering rather precisely. The differential cross section drops rapidly with scattering angle and a shifted forward direction would give asymmetries due to the difference in cross section which would obscure the small polarization effects. Rather than depend on the surveyed alignment of counters, we calculate the location of the 0° direction by fitting a truncated Gaussian to the forward scattering peak. After elasticity selection, the first hodoscope address can be considered to be a label for a subclass of events. A separate 0° direction is calculated for each such subclass, thus implicitly including corrections for stereo effects. Moreover, the Gaussian distribution is separable, and the horizontal and vertical centers may be calculated separately. To improve the statistics, we calculate the horizontal and vertical centers from projections.

The fit is effected with a maximum likelihood method for a one-parameter fit—the mean of the Gaussian. The mean was found to be very insensitive to any reasonable choice of width or truncation points. The width was always set at one channel width and the function was truncated at two channel widths. With this method the center of the scattering distribution can be determined to a few milliradians.

In our coded address hodoscope, the absence of a count in each bit carries essentially the same amount of information as the occurrence of a count. If a bit is lost, the event is not lost but rather is mapped into another address. For this reason inefficiencies are a serious problem in a coded address hodoscope. However, we determine the asymmetry by noting the difference between data with opposite spin directions, so to the extent that the inefficiencies are small and constant they cannot affect the asymmetry to first order. For large asymmetries the second-order effects become important and cannot be ignored. Events which are mapped by inefficiencies show up as a secondary peak apart from the forward scattering peak. Whenever a secondary peak is found, all the data under that peak is rejected.

B. Asymmetries

The intensity for the carbon scattering is given by

$$I(\theta, \phi) = I_0(\theta)[1 + a(\theta) \cos \phi],$$

where I_0 is the unpolarized intensity and a is the asymmetry. Our measurements on the analyzing power of carbon indicate a maximum at a scattering angle of about 6° . We accept data scattered in the angular range $4^\circ < \theta < 8^\circ$. If we integrate over this angular acceptance, we obtain the azimuthal angular dependence:

$$N(\phi) = \int_{4^\circ}^{8^\circ} I(\theta, \phi) d\theta = N_0(1 + \bar{a} \cos \phi).$$

We make a two-parameter fit to the ϕ dependence of the final scattering:

$$N(\phi) = N_0(1 + \epsilon \cos \phi + \delta \sin \phi).$$

This form allows for a more general case where the polarization direction need not be at right angles to the $\phi=0$ reference direction. With this parameterization ϵ is a measure of the left-right asymmetry and δ measures the up-down asymmetry. We can further allow for some nonpolarization ϕ dependence (or biases) by allowing N_0 to become an unspecified function of ϕ .

$$N(\phi) = N_0(\phi)(1 + \epsilon \cos \phi + \delta \sin \phi).$$

We divide the range of ϕ into 12 bins:

$$\begin{aligned} N_j &= \frac{6}{\pi} \int_{(\pi/6)(j-1)}^{(\pi/6)j} N(\phi) d\phi \quad j=1, \dots, 12 \\ &= n_j(1 + \epsilon b_j + \delta c_j). \end{aligned}$$

We separate the bias terms (n_j) by noting that when we reverse the spin direction, the polarization terms (ϵ, δ) change sign while the others do not. For the opposite spin direction

$$N_j^{(\rightarrow)} = n_j(1 - \epsilon b_j - \delta c_j).$$

We are left with a two-parameter fit with 10 degrees of freedom. The asymmetry parameters (ϵ, δ) are fitted to the data with a maximum-likelihood method.

In the limit of infinitely good statistics, our solution for the asymmetries should be independent of the number of bins into which we divide the azimuthal angular range. For those cases of poor statistics or where the $\cos \phi$ form is distorted, we can consider dividing into only two bins—a “right” bin and a “left” bin. Let R =events scattered to the right for spin up, L =events scattered to the left for spin up, R' =events scattered to right for spin down, and L' =events scattered to left for spin down.

The asymmetry is then given by

$$a = \frac{1}{2} \left(\frac{R' - L'}{R' + L'} - \frac{R - L}{R + L} \right).$$

With Poisson statistics, the error is

$$\Delta a = \left[\frac{RL'(R+L') + LR'(L+R')}{(R'+L')(R+L)} \right]^{1/2}.$$

This method for calculating the asymmetry was used in certain special cases.

V. RESULTS AND CONCLUSIONS

A. Polarizations

The asymmetry in the final scattering can be factored as

$$\bar{a} = P_H W \bar{P}_C,$$

where P_H is the beam polarization after the first scatter, \bar{P}_C is the average carbon-analyzing power, and W is a combination of a Wolfenstein parameter and spin-rotation terms. To extract the scattering parameters from our measured asymmetries, we must know the initial p - p polarization and the carbon-analyzing power. We have measured the angular dependence of the carbon polarization from 3° to 7° for energies between 1.0 and 1.55 GeV using a standard double scattering technique. At the upper end of the energy range, the polarizations were found to be quite small. Our results indicate polarizations at 1.55 GeV of about 0.15 ± 0.05 , or asymmetries of 0.02–0.03. The asymmetries were not always reproducible, indicating systematic errors at the 1–2% level. In any event our results seem to exclude polarizations larger than 0.25 at 1.55 GeV.

Such a small analyzing power makes the asymmetry analysis difficult so we decided to compromise on the

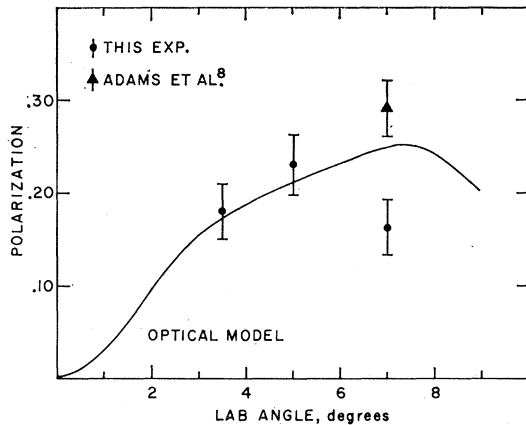


FIG. 6. Carbon-analyzing power at 1 GeV. The solid curve is an optical model prediction based on the accurate lower-energy data of P. G. McManigal, R. D. Eandi, S. N. Kaplan, and B. J. Moyer, *Phys. Rev.* **137**, B620 (1965).

beam energy from the original design, reducing the final scattering energy to 960 MeV. Our measurements at 1 GeV indicate a maximum carbon polarization of 0.23 ± 0.03 . This compares reasonably well with the results of Adams *et al.*,⁸ who find $P_C = 0.29 \pm 0.03$ at 950 MeV and a scattering angle of 7° . These data are plotted in Fig. 6. The average analyzing power is obtained by weighting the polarization by the intensity and averaging over the angular acceptance region:

$$\bar{P}_C = \int_{4^\circ}^{8^\circ} P_C(\theta) I(\theta) d\theta / \int_{4^\circ}^{8^\circ} I(\theta) d\theta.$$

We take $\bar{P}_C = 0.22 \pm 0.03$ for 960 MeV.

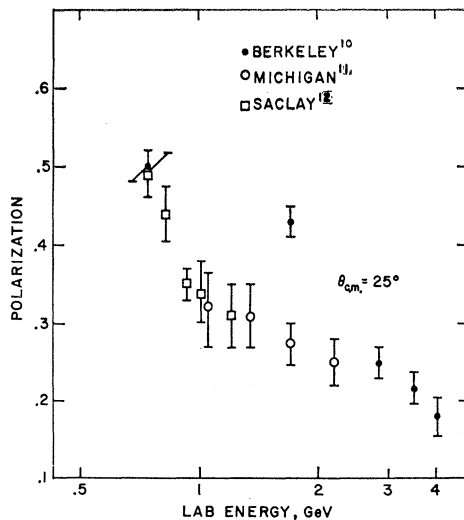


FIG. 7. Proton-proton polarization at 25° in the c.m. system (see Ref. 9).

⁸ C. J. Adams, J. D. Dowell, and G. H. Grayer, *Nuovo Cimento* **51**, A232 (1967).

TABLE I. R -parameter asymmetries.

Run No.	Asymmetry
1	-0.0248 ± 0.0197
2	0.0092 ± 0.0165
3	-0.0086 ± 0.0195
4	0.082 ± 0.040 (incomplete)
Average	0.0064 ± 0.0094

By contrast, p - p polarizations have been extensively measured so we do not measure the initial hydrogen polarization. Figure 7 shows a compilation of recent results⁹⁻¹² as a function of energy for our c.m. scattering angle, $\theta = 25^\circ$. The measurements agree quite well except for a single point at 1.7 GeV. This point has been ignored when interpolating these results to our energy of 2 GeV. After averaging over our angular acceptance, we take the p - p polarization to be $P_H = 0.27 \pm 0.02$ at 2.0 GeV.

As part of our preliminary study of the carbon-analyzing power, we measured the proton-carbon differential cross section with a small target and scintillation-counter telescopes. We compare this measured cross section with the cross section measured by our hodoscope detector for events which scatter in the carbon analyzer. The results are plotted in Fig. 8, where the arbitrary scales have been adjusted to give agreement at the largest angle. The further agreement

TABLE II. A' -parameter asymmetries.

Run No.	Asymmetry
1	-0.0285 ± 0.0156
2	-0.0296 ± 0.0193
3	-0.0146 ± 0.0182
4	-0.0561 ± 0.0187
5	-0.0060 ± 0.0276
Average	-0.0295 ± 0.0085

is an important check that the detector is indeed measuring elastic p -C events.

B. Experimental Asymmetries

The data for each configuration is divided into "runs" consisting of complete cycles of magnet reversals. Each run required about 12 h and contains approximately 10 000 good events for each spin direction, including some 1000 events for an empty target. These 10 000

⁹ Frequently the data of Refs. 10-12 do not measure the p - p polarization precisely at 25° . We have interpolated their results to our scattering angle, but these authors should not be held responsible for our interpolations.

¹⁰ P. Grannis, J. Arens, F. Betz, O. Chamberlain, B. Dieterle, C. Shultz, G. Shapiro, H. Steiner, L. van Rossum, and D. Weldon, *Phys. Rev.* **148**, 1297 (1966).

¹¹ M. J. Longo, H. A. Neal, and O. E. Overseth, *Phys. Rev. Letters* **16**, 536 (1966).

¹² G. Cozzika, Y. Ducros, A. deLesquen, J. Movchet, J. C. Raoul, L. van Rossum, J. Dregel, and J. M. Fontaine, *Phys. Rev.* **164**, 1672 (1967).

events, where a proton elastically scattered from another proton, elastically scatters from the carbon analyzer in the acceptable range of scattering angles, are extracted from a total of about 1 000 000 events selected by the fast logic.

The azimuthal angular distribution for one such run is shown in Fig. 9 along with our maximum-likelihood fit for the asymmetry. The asymmetries for the R -parameter configuration are shown in Table I after correcting for the inelastic background. There are too few runs to justify a χ^2 analysis, but the data for the three runs are seen to be internally consistent.

The asymmetries for the A' -parameter configuration are summarized in Table II. These asymmetries were calculated with the second-analysis method, where the

TABLE III. D -parameter asymmetries.

Run No.	Asymmetry
1 and 2	0.0575 ± 0.0162
3	0.0472 ± 0.0194
Average	0.0533 ± 0.0124

azimuthal angular range is divided into only two bins. The problem arises from a distortion of the $\cos\phi$ asymmetry dependence for this configuration. In order to rotate the final spin direction perpendicular to the beam momentum before analysis, the scattered beam must be bent away from the forward direction. This tends to focus low-momentum, forward-going particles into the detector. The carbon scattering distributions are skewed in the vertical direction because of the low-momentum tail. This skewness distorts the $\cos\phi$ dependence, so that the cosine fits give a large χ^2 . However, since the effect is strictly in the vertical direction, it should have little effect on the left-right fit. The cosine fits are consistent with the solutions of a left-right fit, but the errors are much larger because of the poor fit.

The results for the D configuration are given in Table III. Data for the first two runs have been combined to average out the effects of an apparent bias. The remaining bias after combination of the two runs is less than 0.002.

The Wolfenstein parameters R , A' , and D are calculated from these asymmetries using our values for the hydrogen polarization and carbon-analyzing power and including correction terms for spin rotations. The results for the parameters are shown in Table IV.

TABLE IV. Wolfenstein parameters.

Parameter name	Asymmetry	Spin-rotation correction	Parameter value
R	0.0064 ± 0.0094	0.978	0.11 ± 0.16
A'	-0.0295 ± 0.0084	0.911	-0.54 ± 0.16
D	0.0533 ± 0.0124	0.988	0.91 ± 0.21

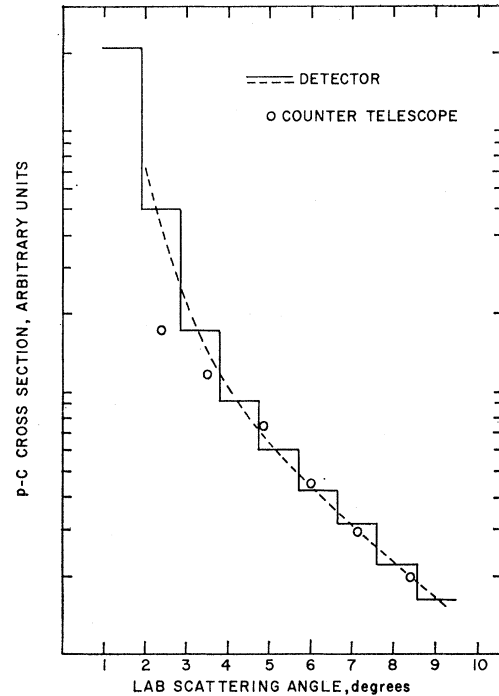


FIG. 8. Proton-carbon differential cross section at 1 GeV. The dashed line is meant to suggest a smooth form of the detector histogram.

C. Interpretation

In general, the three measured parameters do not define a unique solution for the five real numbers which characterize the scattering matrix. We must rely on specific models to interpret our results. We can assume a model, use the model to calculate the three amplitudes, and then compare with our results for consistency. Such models are also useful in developing a physical picture of the interaction.

Our results are compared with the predictions of three very simple models in Table V. These models will

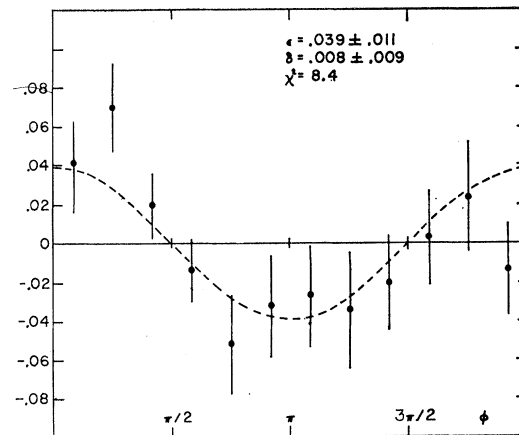


FIG. 9. Azimuthal angular distribution of the asymmetry for protons elastically scattered by the carbon analyzer.

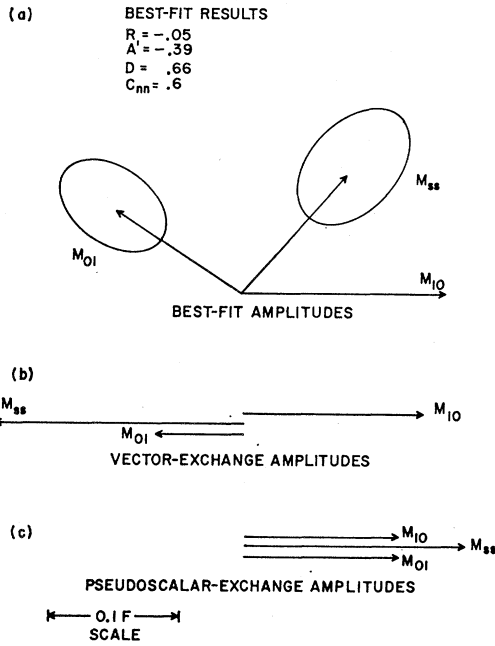


FIG. 10. (a) Minimal- χ^2 solution for spin amplitudes. (b) Helicity conservation limit for single vector-meson-exchange spin amplitudes. (c) Helicity reversal limit for single pseudoscalar-meson-exchange spin amplitudes.

be discussed in order. The “black hole” model is trivial in that it predicts no spin coupling. We envision a spherically symmetric absorptive region in the spirit of a diffraction model with no ad hoc spin-orbit terms. Clearly with no spin effects, we could observe no asymmetries: All the Wolfenstein parameters must vanish. This simple model is not consistent with the data. The two remaining models are concerned with the exchange of a single meson.¹³ The first is a “helicity reversal,” or single pseudoscalar-meson-exchange model. The familiar one-pion exchange which is known to work well at small momentum transfers fits this model. The A' parameter is seen to be consistent with pseudoscalar-meson exchange, but neither R nor D agree with the pseudoscalar-meson prediction.

Finally, we consider the “helicity conservation” or single vector-meson exchange. We must take a relativistic limit ($p^2 \gg m^2$) to obtain the simple helicity-conservation relations from a vector-meson exchange. The experimental results do not agree with the single vector-meson-exchange predictions for any of the parameters. If we do not take the relativistic limit, the

¹³ A. Scotti and D. Y. Wong, Phys. Rev. **138**, B145 (1965).

TABLE V. Comparison of results with model predictions.

Parameter	Experimental value	“Black hole” model	Pseudoscalar-meson exchange ^a	Vector-meson exchange ^a
R	0.11 ± 0.16	0	—	4/9
A'	-0.54 ± 0.16	0	—	8/9
D	0.91 ± 0.21	0	—	4/9

^a Reference 13.

discrepancy is even larger. We must conclude that none of the three simple models considered can account for the data.

Although the three measured parameters do not uniquely define the scattering matrix, the functional forms for the amplitude dependence of D , R , and A' imply strong constraints on the amplitudes. One of the five real numbers which characterize the scattering matrix is dimensional and fixes the scale for the amplitudes. This number is set by the differential cross section. The other four dimensionless numbers are fit to the three measured Wolfenstein parameters, and a unique minimal χ^2 fit is obtained. The best-fit solution is shown in Fig. 10. The minimum χ^2 value, $\chi^2 = 3.3$, indicates that our measured parameters are consistent at the limit of the statistical errors. The error ellipses in Fig. 10 were obtained by varying the four parameters one at a time from the minimum χ^2 solution. The errors thus obtained should not be considered as independent for simple error propagation; they are strongly correlated.

The solution of Fig. 10 uniquely defines the scattering matrix and thus permits calculation of any parameter of interest. In particular, it implies that the spin-correlation parameter C_{nn} is equal to 0.6. This agrees with the values (but not the trend) observed recently at slightly lower energies by Cozzika *et al.*¹²

In summary, we conclude on the basis of our measurements of D , R , and A' that spin effects are still important in the nucleon-nucleon interaction at 2 GeV. A simple one-meson-exchange model cannot account for our results for either pseudoscalar- or vector-meson exchange. It would seem that the transformation properties of the strong interaction still do not approach a simple limit at four-momentum transfers $-t = 1.8$ (GeV/c)².

ACKNOWLEDGMENTS

It is a pleasure to thank the operations and floor crew of the Cosmotron for their efficient machine operation during the experiment. We are indebted to Mr. J. Lypecky for his help in assembling the experiment.